ACS OMEGA

Open Access

http://pubs.acs.org/journal/acsodf

Article

Theoretical Study of Efficient Photon−Phonon Resonance Absorption in the Tungsten-Related Vibrational Mode of Scheelite

Yi Yin, Yi-Ning Li, Sicheng Liu, Yan Jiang, Xiao-Yan Liu, and Peng Zhang*

Cite This: *ACS Omega* 2024, 9, 10517−10521

Read Online

ACCESS | Metrics & More | Article Recommendations | Supporting Information

ABSTRACT: Tungsten (W) is an extremely rare and vital metal extensively used in metallurgy, the chemical industry, optoelectronic devices, and machinery manufacturing. In this work, an environmentally friendly and efficient physical method based on photon−phonon resonance absorption (PPRA) is proposed for separating W from scheelite. We calculated the vibrational spectrum of calcium tungstate ($CaWO_4$) and assigned the infrared (IR) absorption and Raman scattering peaks through a dynamic analysis of the normal modes. We focused on the strong IR absorption peaks related to W and identified three high-intensity IR-active modes at around 830 cm^{-1}, corresponding to the stretching of the W−O bonds. Therefore, we propose the use of high-power terahertz (~25 THz) laser radiation to facilitate W extraction from compounds, leveraging the high efficiency of PPRA. Experimental testing is required to determine the precise absorption frequency under industrial production conditions.

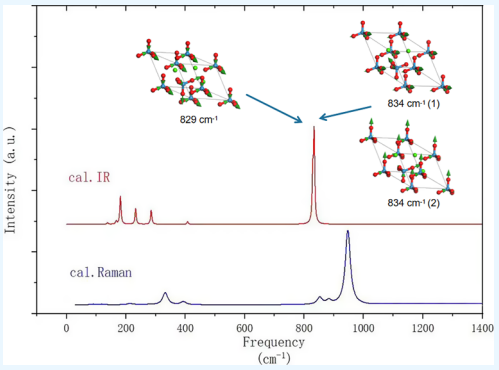

1. INTRODUCTION

Tungsten (W) is a rare and essential element and has the highest melting point among the refractory metals. Moreover, it possesses excellent high-temperature strength and good corrosion resistance to molten alkali.[1] W is extensively applied in several fields, including metallurgy, the chemical industry, optoelectronic devices, and the machinery industry.[2] In particular, W has vital applications in quantum electronics, medical treatments, and military product manufacturing.[3−6] With the development of machinery, automobile, national defense, and electronics industries in China and the continuous progress of hard-alloy and W processing technology, the consumption of raw W in China has grown rapidly. Between 1990 and 2019, consumption increased from 10,000 tons to 48,000 tons, representing an average annual growth rate of 5.5%. The global demand for W is expected to reach 110,000 tons by 2025.[7,8] However, the W content in the earth's crust is relatively low, 0.001%. In 2016, the global reserve of W was 3.1 million tons with a basic reserve at 6.2 million tons, making W an extremely rare resource. China's W reserve was 1.9 million tons with a basic reserve of 4.2 million tons. China possesses 61% of the world's W reserves, establishing it as the country with the largest W reserve globally.

Tungsten is predominantly found in various types of rocks in the forms of wolframite and scheelite, making it challenging to extract. The primary component of scheelite is calcium tungstate ($CaWO_4$), a critical and commonly used material in W production. Consequently, we conducted a spectral analysis of $CaWO_4$ to identify an efficient method for W separation. Typically, W can be separated and extracted through organic solvent extraction and ion exchange methods.[9,10] In China, the primary methods for smelting wolframite involve NaOH leaching and Na_2CO_3 sintering following water leaching, while alkali dissolution following hydrochloric acid decomposition is commonly employed for scheelite smelting. Additional techniques such as hot ball milling,[11] alkali pressure boiling,[12,13] and sulfur and phosphorus mixed acid leaching[14,15] have been developed. W recovery methods include zinc melting[15] and selective electrochemical dissolution.[16] Although numerous W extraction methods exist, they often lead to W pollution in air, water, and soil. Soil contamination with W is a significant concern, as W can interact with the environmental medium, posing a threat to both the ecological environment and human health.[17,18] In China, research on W pollution characteristics and prevention technologies remains relatively limited. Consequently, there is an urgent need for a novel, environmentally friendly technology for extracting W from ore with minimal pollution and higher efficiency suitable for large-scale industrial production.

Numerous spectroscopic studies have focused on $CaWO_4$, a crucial and common material in W production.[19−21] Basiev et al. studied $CaWO_4$ via Raman spectroscopy.[22] Ryu et al.

Received: October 31, 2023
Revised: January 20, 2024
Accepted: February 8, 2024
Published: February 20, 2024

measured the Raman spectrum and ultraviolet−visible spectrum of $CaWO_4$ nanoparticles collected from a colloidal suspension.[3] Additionally, Golubovic et al. grew $CaWO_4$ and Nd:$CaWO_4$ (0.8% Nd) single crystals from melts through the Czochralski technique and measured the infrared (IR) spectra of Nd:$CaWO_4$ and $CaWO_4$ single crystals at both room and liquid nitrogen temperatures.[23]

Despite the aforementioned experimental and spectroscopic studies of $CaWO_4$, there remains a lack of theoretical research on its lattice dynamic processes and the assignment of IR and Raman spectra peaks for $CaWO_4$. In this study, we simulated the vibrational spectrum of $CaWO_4$ and compared it with the experimental spectrum to accurately assign the Raman and IR peaks. It is worth noting that the Raman spectrum we calculated was in the IR region so it was nonresonant Raman spectrum. Based on the IR-active peaks related to W, we propose a new method to enhance the separation process of W from oxide, namely photon−phonon resonance absorption (PPRA).[24,25]

2. SIMULATION METHOD

$CaWO_4$ has a crystal structure of the scheelite type with C_{4h} point-group symmetry and $I4_1/a$ space-group symmetry. In this structure, Ca^{2+} ions occupy 4b Wyckoff positions (0, 1/4, and 5/8) with local symmetry, while W^{6+} ions occupy 4a Wyckoff positions (0, 1/4, and 1/8) with the same local symmetry. W^{6+} ions are tetrahedrally coordinated to O^{2-} ions, with a coordination number of 4, while Ca^{2+} ions are in distorted hexahedral coordination with O^{2-} ions, with a coordination number of 8.[26] Vibrational spectral simulations of the $CaWO_4$ crystal were performed using a primitive cell that contained two $CaWO_4$ molecules.

We performed geometry optimization and phonon calculations using first-principle density-functional theory (DFT) and the Cambridge Serial Total Energy Package (CASTEP)[27] code. To account for electron density fluctuations in $CaWO_4$, we adopted the generalized gradient approximation of the Perdew−Burke−Ernzerhof (PBE) exchange correlation functional, which was semilocalized and provided more accurate descriptions of energy and structure. It exhibited better consistency with experimental results compared with other functionals.[28] The convergence tolerance values for energy and the self-consistent field were set to 1×10^{-9} eV/atom. An energy cutoff of 800 eV and a $3 \times 3 \times 4$ k-point mesh were applied. Furthermore, because of the large number of electrons in 5d metal W, we employed norm-conserving pseudopotential, which packages the core electrons and the nucleus together to balance the accuracy and the time, and finite displacement was used for phonon calculations. Additionally, optical ($\omega = \infty$) and dc ($\omega = 0$) dielectric permittivity, optical ($\omega = \infty$), and static ($\omega = 0$) molecular polarizability were calculated in this work, allowing us to obtain simulated IR and Raman spectra. According to the calculated data, we assigned the vibrational spectra through a dynamic process analysis of each wavenumber. Consequently, we were able to identify W-related peaks in these spectra and determine the highest IR absorption peaks in terms of W-related PPRA.

3. RESULTS AND DISCUSSION

There are 12 atoms in one $CaWO_4$ primitive cell and 33 (i.e., $[12 \times 3] - 3$, subtracting 3 for the acoustic normal modes) optical normal modes, which can be examined through IR absorption and Raman scattering via phonon−photon coupling. Owing to the symmetric structure of $CaWO_4$, changes in the dipole moment and polarizability of the primitive cell are mutually repulsive, resulting in entirely complementary IR-active and Raman-active modes. Figure 1 illustrates the simulated IR and Raman spectra.

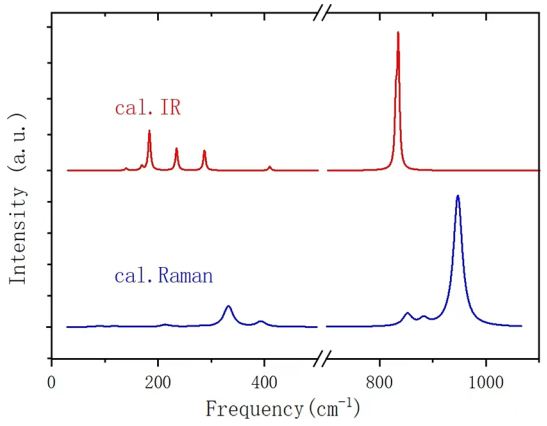

Figure 1. Simulated IR absorption and Raman scattering spectra. Mp = 1 × 1.0. The main peaks are almost complementary.

Table 1 compares the calculated wavenumbers and the experimental IR and Raman peaks. The assignments for the 33 vibrational modes are given in the last column. We identify 18 Raman-active vibrational modes, including four wavenumbers (109, 178, 244, and 839 cm^{-1}) that are doubly degenerate, and 12 IR-active vibrational modes, which also feature four wavenumbers (138, 181, 285, and 834 cm^{-1}) that are doubly degenerate. However, the modes at 254, 410, and 942 cm^{-1} exhibit neither IR nor Raman activity. According to group theory, the 36 degrees of freedom of a $CaWO_4$ primitive cell are divided into 26 species of vibrational modes $3A_g+5A_u+5B_g+3B_u+5E_g+5E_u$, where the species E vibrations are doubly degenerate. Among these vibrational modes, $3A_g$, $5B_g$, and $5E_g$ are Raman-active modes; $4A_u$ and $4E_u$ are IR-active modes; $3B_u$ are silent modes; and $1A_u$ and $1E_u$ are acoustic modes.[20] Compared with the reported experimental results, the simulated peaks show a small blue shift (about 10 cm^{-1}). This can validate the theoretical methodology employed in our work.

In the lowest-vibrational-energy region, we assigned the three vibrational modes at 86 and 109 cm^{-1} to WO_4^{2-} translations in which the two anions vibrate relatively along three orthogonal directions. The two vibrational modes at 109 cm^{-1} are degenerate. The mode at 86 cm^{-1} is shown in Figure 2 as an example of the WO_4^{2-} translation. The anions at the eight apex angles represent one anion in a primitive cell and the other one is in the primitive cell. The two degenerate modes at 138 cm^{-1} belong to the $(WO_4)^{2-}$ rotation. Lim detected peaks at 115−211 cm^{-1} and assigned them to interion vibrations, in which the two ionic groups vibrated together.[29] Porto and Scott reported that the E_u mode at 125−150 cm^{-1} was related to interion vibration, and the E_u mode at 150−200 cm^{-1} was associated with rotation.[20] The tentative assignments of the modes were based on group theory, whereas our assignments are based on first-principle calculations.

We assigned the six modes at 167, 178, 181, and 204 cm^{-1} to Ca^{2+} translations. We present the mode at 181 cm^{-1} as a typical Ca^{2+} translation of the IR activity (Figure 3). Ryu et al.

https://doi.org/10.1021/acsomega.3c08636
ACS Omega 2024, 9, 10517−10521

Table 1. Comparisons of 33 Calculated Wavenumbers (IR and Raman Activities Are Listed) of $CaWO_4$ with Experimental Data (Unit cm^{-1})

wavenumbers	activity	IR exp.	Raman exp.	assignment
86	Raman		84[a], 86[b], 84[c]	WO_4^{2-} translation
109	Raman		117[a], 118[b], 117[c]	WO_4^{2-} translation
109	Raman			WO_4^{2-} translation
138	IR	143[a], 143[b]		WO_4^{2-} rotation
138	IR			WO_4^{2-} rotation
167	IR			Ca^{2+} translation
178	Raman		180[b], 185[d]	Ca^{2+} translation
178	Raman			Ca^{2+} translation
181	IR	180[a], 180[b]		Ca^{2+} translation
181	IR			Ca^{2+} translation
195	Raman		195[a], 196[b]	WO_4^{2-} rotation
204	Raman		210[a], 210[b], 212[c], 210[d]	Ca^{2+} translation
232	IR	237[a], 237[b]		WO_4^{2-} rotation
244	Raman			WO_4^{2-} rotation
244	Raman			WO_4^{2-} rotation
254				WO_4^{2-} rotation
285	IR	275[a], 309[b]		WO_4^{2-} rotation
285	IR			WO_4^{2-} rotation
315	Raman			WO_4^{2-} bending
316	Raman		336[a], 334[b], 334[c]	WO_4^{2-} bending
374	Raman			WO_4^{2-} bending
378	Raman		403[b], 401[c]	WO_4^{2-} bending
378	Raman			WO_4^{2-} bending
408	IR	409[a], 435[b], 439[c], 433[d]		WO_4^{2-} bending
410				WO_4^{2-} bending
829	IR	797[a], 793[b], 754[c]		WO_4^{2-} stretching
834	IR	822[c], 862[d]		WO_4^{2-} stretching
834	IR			WO_4^{2-} stretching
839	Raman		838[a], 838[b], 839[c]	WO_4^{2-} stretching
839	Raman			WO_4^{2-} stretching
873	Raman			WO_4^{2-} stretching
939	Raman		912[a], 922[b], 912[c]	WO_4^{2-} stretching
942				WO_4^{2-} stretching

[a]Ref 20. [b]Ref 30. [c]Ref 34. [d]Ref 26.

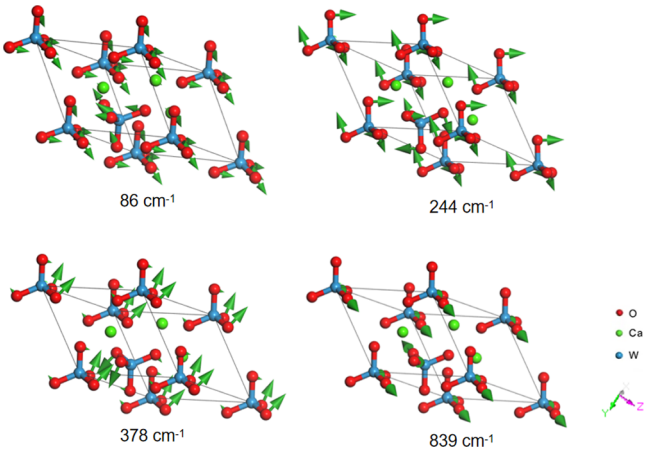

Figure 2. Four typical Raman-active vibrational modes. The mode of wavenumber at 86 cm^{-1} represents anion translation, in which the two anion groups in one primitive cell vibrate in opposite directions. The mode at 244 cm^{-1} represents WO_4^{2-} rotation, the mode at 378 cm^{-1} represents WO_4^{2-} bending, and the mode at 839 cm^{-1} represents O−W stretching.

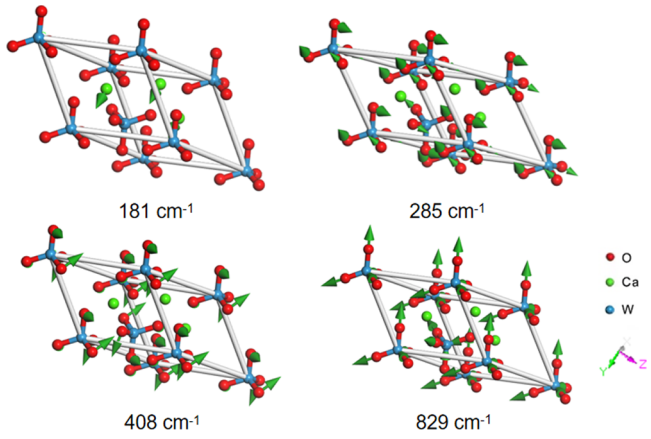

Figure 3. Four typical IR-active vibrational modes. The mode at 181 cm^{-1} corresponds to Ca^{2+} translation, the mode at 285 cm^{-1} corresponds to WO_4^{2-} rotation, the mode at 408 cm^{-1} corresponds to WO_4^{2-} bending, and the mode at 829 cm^{-1} corresponds to O−W−O stretching.

suggested that the bands at 185 cm^{-1} are related to the translational mode of the Ca−O bond in $CaWO_4$.[3] Russell assigned modes with frequencies below 435 cm^{-1} to vibrations between the loosely bound Ca^{2+} and WO_4^{2-} ions.[30] Zhang et al. reported that the Raman peaks in the range of 100−250 cm^{-1} corresponded to the contraction and bending vibrations of the CaO_8 groups.[31]

We propose that the six modes at 232−285 cm^{-1} correspond to WO_4^{2-} rotations. Additionally, seven modes at 315−410 cm^{-1} correspond to WO_4^{2-} bending vibrations. The modes at 244 and 378 cm^{-1} are demonstrated in Figure 2, while the modes at 285 and 408 cm^{-1} are shown in Figure 3. Ryu et al. assigned the bands at 210 cm^{-1} to the translational

https://doi.org/10.1021/acsomega.3c08636
ACS Omega 2024, 9, 10517−10521

mode of the anion group.[3] However, we disagree with their assignment because the anion group has a greater mass than Ca^{2+}. Lv et al. suggested that vibrational peaks within the range of 350−600 cm^{-1} were related to W−O stretching vibrations.[32] However, as shown in Table 1, the lowest wavenumber for W−O stretching is 829 cm^{-1}. Zhang et al. reported that Raman peaks at 334 and 405 cm^{-1} corresponded to the symmetric and nonsymmetric bending vibrations of WO_4^{2-}, respectively, which aligns with our calculations.[31] Furthermore, Abozaid et al. examined the IR spectroscopy of single crystals of calcium tungstate doped with neodymium ($CaWO_4$:Nd^{3+}). They reported a weak vibration band at 436 cm^{-1}, related to W−O bending vibration, and a weak but sharp band at 433 cm^{-1}, related to the Ca−O bond.[26] Similarly, Phuruangrat et al. detected a weak W−O vibration at 433 cm^{-1}.[33]

In the high-frequency vibrational region, eight modes at 829−942 cm^{-1} correspond to intra-anion WO_4^{2-} stretching. These kinds of vibrations are related to the O−W bond stretching. Two examples of modes at 829 (IR-active) and 839 cm^{-1} (Raman-active) are presented in Figures 3 and 2, respectively. Ryu et al. reported that the $\nu 3$ (B_g) vibration was located around 840 cm^{-1}, and the $\nu 3$ (E_g) vibration was found at 800 cm^{-1}.[3] Russell assigned modes with wavenumbers of 778−922 cm^{-1} to the internal vibrations of tightly bound WO_4^{2-} ions.[30] Furthermore, Zhang et al. reported that Raman peaks at 910, 836, and 797 cm^{-1} corresponded to the stretching vibration of WO_4^{2-}, and the mode at 910 cm^{-1} was related to the symmetric stretching vibration of WO_4^{2-}.[31] Abozaid et al. reported an IR absorption band in $CaWO_4$:Nd^{3+} at around 742 cm^{-1} and a strong band at 862 cm^{-1}, attributing them to the O−W−O stretching.[26] Similarly, Phuruangrat et al. detected strong antisymmetric W−O stretching in WO_4^{2-} tetrahedrons in the range of 711−933 cm^{-1}.[33] Although the region above 800 cm^{-1} is associated with W−O stretching, the intensities of IR and Raman photon−phonon coupling are different owing to different physical mechanisms.

According to the calculation results, three IR-active modes at 829 and 833 cm^{-1} exhibit the strongest intensities, as illustrated in Figure 1, while the largest Raman peak is at 939 cm^{-1}. For the dynamic processes of the three IR-active modes, see the Supporting Information Movies. Considering that IR absorption is due to the PPRA effect, the experimental peaks at around 830 cm^{-1} feature the most efficient photon−phonon absorption. Two experimental peaks occur at approximately 822 and 862 cm^{-1}.[26,34] Accurate IR absorption experiments in this region will be necessary in the future. Applying a high-power terahertz laser to a $CaWO_4$ crystal will endow the phonons of the W−O vibrational mode with high energy-absorption efficiency, which may facilitate chemical bond breakage and W separation from $CaWO_4$. This could offer a novel physical method for W separation without chemical pollution. Figure 4 presents the charge distribution between W and O. The oxygen shows a quite electronegative with a small charge distribution around W. This shows that the W−O bond possesses a high property of ionic bond, which reduces the strength of the W−O bond. Therefore, it is possible to achieve a W−O bond break through PPRA.

4. CONCLUSIONS

According to first-principle DFT simulations, we analyzed the dynamic processes of the vibrational modes of $CaWO_4$ and identified Raman-active and IR-active vibrational modes. New assignments that were not present in experimental data are presented.

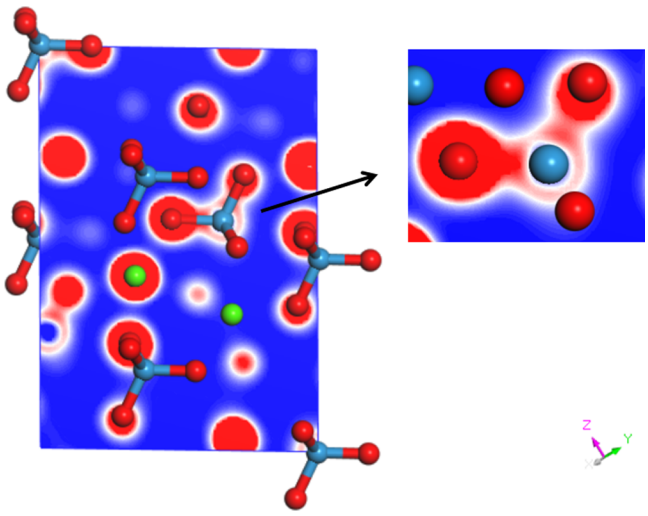

Figure 4. Electron density at a certain slice. The red color represents a large electron density, and the blue color represents a small electron density.

In our analysis of vibrational modes, we focused on the W-related vibrational modes. Experiments and simulations revealed that three W−O stretching vibrational modes with wavenumbers around 830 cm^{-1} corresponded to high-intensity experimental peaks, which indicates efficient absorption in IR spectroscopy. Given that the physical mechanism of IR spectroscopy is PPRA, we propose the use of a high-power terahertz laser radiation (at ∼25 THz) on the $CaWO_4$ crystals. The resonance absorption is expected to facilitate the breaking of W−O bonds. This may offer an environmentally friendly and effective method for separating W from scheelite. Additional experimental testing is required to determine the precise frequency at which the high-power terahertz laser should operate when it is applied to $CaWO_4$ crystals.

■ ASSOCIATED CONTENT

Supporting Information

The Supporting Information is available free of charge at https://pubs.acs.org/doi/10.1021/acsomega.3c08636.

IR-active vibrational mode at 829 cm^{-1} (MP4)
IR-active vibrational mode-1 at 834 cm^{-1} (MP4)
IR-active vibrational mode-2 at 834 cm^{-1} (MP4)

■ AUTHOR INFORMATION

Corresponding Author

Peng Zhang − *School of Space Science and Physics, Shandong University, Weihai 264209, China;* orcid.org/0000-0002-1099-6310; Email: zhangpeng@sdu.edu.cn

Authors

Yi Yin − *School of Space Science and Physics, Shandong University, Weihai 264209, China*

Yi-Ning Li − *School of Space Science and Physics, Shandong University, Weihai 264209, China*

Sicheng Liu − *School of Space Science and Physics, Shandong University, Weihai 264209, China*

Yan Jiang − *School of Space Science and Physics, Shandong University, Weihai 264209, China*

https://doi.org/10.1021/acsomega.3c08636
ACS Omega 2024, 9, 10517−10521

Xiao-Yan Liu − *School of Space Science and Physics, Shandong University, Weihai 264209, China*

Complete contact information is available at: https://pubs.acs.org/10.1021/acsomega.3c08636

Notes

The authors declare no competing financial interest.

■ ACKNOWLEDGMENTS

We are grateful to the project ZR2022MA017 supported by Shandong Provincial Natural Science for financial support. The numerical calculations were performed on the supercomputing system at the Supercomputing Center, Shandong University, Weihai.

■ REFERENCES

(1) Zoroddu, M. A.; Medici, S.; Peana, M.; Nurchi, V. M.; Lachowicz, J. I.; Laulicht-Glick, F.; Costa, M. Tungsten or Wolfram: Friend or Foe? *Curr. Med. Chem.* **2018**, *25* (1), 65−74.

(2) Thongtem, T.; Phuruangrat, A.; Thongtem, S. Characterization of MeWO4 (Me = Ba, Sr and Ca) nanocrystallines prepared by sonochemical method. *Appl. Surf. Sci.* **2008**, *254* (23), 7581−7585.

(3) Ryu, J. H.; Park, G. S.; Kim, K. M.; Lim, C. S.; Yoon, J.-W.; Shim, K. B. Synthesis of CaWO4 nanocolloidal suspension via pulsed laser ablation and its optical properties. *Appl. Phys. A: Mater. Sci. Process.* **2007**, *88* (4), 731−736.

(4) Johnson, L. F.; Boyd, G. D.; Nassau, K.; Soden, R. R. Continuous operation of a solid-state optical maser. *Phys. Rev.* **1962**, *126* (4), 1406.

(5) Yuan, X.; Xiao, T.; Huang, Q.; Ren, S.Environmental toxicity and pollution prevention techniques of tungsten: a review. *Environ. Pollut. Control* **2022**, *44*, 9.

(6) Koutsospyros, A.; Braida, W.; Christodoulatos, C.; Dermatas, D.; Strigul, N. A review of tungsten: from environmental obscurity to scrutiny. *J. Hazard Mater.* **2006**, *136* (1), 1−19.

(7) Tang, P.; Wang, S.; Wang, J. Historical Analysis and Demand Forecast of Global Tungsten Consumption. *Nat. Resour. Econ. China* **2021**, *34* (01), 55−59.

(8) Yu, Z. Current Situation Analysis and Suggestions of Tungsten Industry in China. *Land Resour. Inform. J.* **2020**, *10*, 6.

(9) Wang, M. The Latest Development of Ion Exchange Technology in Tungsten Smelting. *Rare Metals Cemented Carbides* **2013**, *41* (06), 13−16.

(10) Li, H.-G.; Liu, M.-S.; Sun, P.-M.; Li, Y.-J.; Su, P.-T. Introduction of a New Achievement: Processing and Equipment of Caustic Decomposition of Low-grade Scheelite and Scheelite-wolframite Mixed Concentrates. *Bull. Natl. Nat. Sci. Found China* **1997**, *3*, 210−212.

(11) He, L.-H.; L, X.-H.; Zhao, Z.-W.; Liang, Y. Theory and technology on the alkali decomposition of tungsten ores. *China Tungsten Ind.* **2012**, *27* (02), 22−27.

(12) Li, H.-G.; Li, Y.-J.; Sun, P.-M.; Liu, M.-S. Studies on the inhibition of impurities in caustic decomposition of tungsten concentrates. *Eng. Sci.* **2000**, *2*, 59−61.

(13) Zhao, Z.; Liang, Y.; Liu, X.; Chen, A.; Li, H. Sodium hydroxide digestion of scheelite by reactive extrusion. *International Journal of Refractory Metals & Hard Materials* **2011**, *29* (6), 739−742.

(14) Yang, K.; Zhang, W.; He, L.; Li, Y.; Guo, F.; Chen, X.; Li, J.; Liu, X.; Zhao, Z. Leaching kinetics of wolframite with sulfuric-phosphoric acid. *Chin. J. Nonferr. Metals* **2018**, *28* (1), 175−182.

(15) Kuang, H. The Latest Development of Waste Cemented Carbide Recovery with Zinc Melting Method. *Rare Metals Cemented Carbides* **2016**, *44* (5), 79−82.

(16) Ren, H.; Tang, Z.; Liu, X. Progress in Hydrometallurgy Process of Tungsten. *Rare Metals Cemented Carbides* **2019**, *47* (3), 1−8.

(17) Shi, M.; Tang, Z.-Y.; Chen, X.-Y.Current and Future Development of Waste water Treatment from Modern Tungsten Metallurgical Process. *Rare Metals Cemented Carbides* **2015**, *43*, 2.

(18) Ma, B.; Du, B.Y.; Yan, X. F.; Kang, G. D. Hazardous Characteristics and Mechanical Properties of Vitrification Product of Tungsten Slag. *J. Ecol. Rural Environ.* **2021**, *37* (09), 1218−1224.

(19) Silva, M. S.; Jesus, L. M.; Barbosa, L. B.; Ardila, D. R.; Andreeta, J. P.; Silva, R. S. Crucible less crystal growth and Radio luminescence study of calcium tungstate single crystal fiber. *Opt. Mater.* **2014**, *37*, 51−54.

(20) Porto, S. P. S.; Scott, J. F. Raman Spectra of CaWO4, SrWO4, CaMoO4, and SrMoO4. *Phys. Rev.* **1967**, *157* (3), 716−719.

(21) Burcham, L. J.; Wachs, I. E. Vibrational analysis of the two non-equivalent, tetrahedral tungstate (WO4) units in Ce2(WO4)3 and La2(WO4)3. *Spectrochim. Acta* **1998**, *54* (10), 1355−1368.

(22) Basiev, T. T.; Sobol, A. A.; Voronko, Y. K.; Zverev, P. G. Spontaneous Raman spectroscopy of tungstate and molybdate crystals for Raman lasers. *Opt. Mater.* **2000**, *15* (3), 205−216.

(23) Golubovic, A.; Gajic, R.; Dohcevic-Mitrovic, Z.; Nikolic, S. Nd pronounced anharmonicity in IR spectra of CaWO4 single crystals. *Science of Sintering* **2006**, *38* (3), 265−272.

(24) Li, M. M.; Cao, J. W.; Qin, X. L.; Liu, X. Y.; Yuan, X. Q.; Dong, X. T.; Guo, Q.; Sun, Y.; Zhang, P. Theoretical Prediction of Rhenium Separation from Ammonium Perrhenate by Phonon-Photon Resonance Absorption. *ACS Omega* **2022**, *7* (6), 5437−5441.

(25) Guo, Q.; Liu, X. Y.; Liu, S. C.; Li, Y. N.; Yin, Y.; Zhang, P. A theoretical analysis of the vibrational modes of ammonium metavanadate. *RSC Adv.* **2023**, *13* (23), 15975−15980.

(26) Abozaid, R.; Lazarevic, Z.; Radojevic, V.; Rabasovic, M.; Sevic, D.; Rabasovic, M.; Romcevic, N. Characterization of neodymium doped calcium tungstate single crystal by Raman, IR and luminescence spectroscopy. *Science of Sintering* **2018**, *50* (4), 445−455.

(27) Clark, S. J.; Segall, M. D.; Pickard, C. J.; Hasnip, P. J.; Probert, M. J.; Refson, K.; Payne, M. C. First principles methods using CASTEP. *Zeitschrift Fur Kristallographie* **2005**, *220* (5−6), 567−570.

(28) Perdew, J. P.; Burke, K.; Ernzerhof, M. Generalized gradient approximation made simple (vol 77, pg 3865, 1996). *Phys. Rev. Lett.* **1997**, *78* (7), 1396−1396.

(29) Lim, C. S. Synthesis and Spectroscopic Properties of Superparamagnetic Iron Oxide Nanoparticle/ CaWO4:Er3+, Yb3+ Composites by Microwave-Assisted Metathetic Method. *Asian J. Chem.* **2014**, *26* (5), 1297−1300.

(30) Russell, J. P.; Loudon, R. The first-order Raman spectrum of calcium tungstate. *Proc. Phys. Soc.* **1965**, *85*, 1029 DOI: 10.1088/0370-1328/85/5/321.

(31) Zhang, S.; Lv, L.; Wang, H.; Zhu, C.; Pang, R.; Feng, J.; Li, D.; Liu, G.; Jiang, L.; Li, C. Structure and luminescence properties of CaWO4-EuMO4 (M = Nb, Ta) solid solution. *J. Lumin.* **2019**, *211*, 183−192.

(32) Lv, J.; Xiao, E.-C.; Li, X.-H.; Dong, X.; Chen, Y.; Yue, Z.; Shi, F. Crystal structures, dielectric properties, and lattice vibrational characteristics of (1-x)CaWO4-xTiO2 composite ceramics. *Ceram. Int.* **2020**, *46* (3), 3715−3724.

(33) Phuruangrat, A.; Thongtem, T.; Thongtem, S. Synthesis, characterisation and photoluminescence of nanocrystalline calcium tungstate. *Journal of Experimental Nanoscience* **2010**, *5* (3), 263−270.

(34) Cho, S.-W. Pycnometric and Spectroscopic Studies of Red Phosphors Ca2+(1−1.5x)WO4:Eu3+xand Ca2+(1−2x)-WO4:Eu3+x,Na+x. *Bulletin of the Korean Chemical Society* **2013**, *34* (9), 2769−2773.